CrossMark

ORIGINAL PAPER

Preparation and characterization of biodegradable polyurethanes composites filled with silver nanoparticles-decorated graphene

Cheng-Lung Wu[1] · Chih-Yuan Tsou[1] · Yen-Chun Tseng[1] · Hsun-Tsing Lee[2] ·
Maw-Cherng Suen[3] · Jia-Hao Gu[1] · Chi-Hui Tsou[4,5] · Shih-Hsuan Chiu[1]

Abstract In this study, polyurethane (PU) was synthesized using 4,4,-diphenylmethane diisocyanate (MDI) as a hard segment, polycaprolactone diol (PCL) as the soft segments and 1,4-butandiol (1,4-BD) as a chain extender. Nanosilver/graphene (Ag/G) was added to the PU matrix to prepare Ag/G/PU nanocomposites. EDS, SEM and XRD are used for assaying the silver content and characterization of Ag/G. TEM, FT-IR, XRD and EDS were used to characterize the structure and morphology of the Ag/G/PUs nanocomposites. The TEM results show that Ag/G belongs to sheet structures and is dispersed in a PU matrix. The SEM showed that the strong interfacial adhesion between the Ag/G and PU is indicated. FT-IR spectra analysis shows that the functional group of PU is free of obvious changes by adding a small amount of Ag/G in the PU matrix. XRD results showed that the main crystalline peak (26°) of Ag/G became more apparent with increasing content of Ag/G, and EDS showed that the content of Ag increased with increasing content of Ag/G in the Ag/G/PUs nanocomposites. The thermal stability and mechanical properties of Ag/G/PUs nanocomposites are improved with increasing content of Ag/G. Contact angle and AFM results showed that the hydrophobicity and surface roughness increased with increasing content of Ag/G. Moreover, the Ag/G/PUs nanocomposites exhibit antibacterial activities toward *Staphylococcus aureus* as well as *Escherichia coli* and their antibacterial rates increase with increasing Ag/G. In addition, the electrical conductivity measurements showed that both surface and volume resistance of the Ag/G/PUs nanocomposites decreased as the amount of Ag/G increased.

Keywords Polyurethane · Nanosilver · Graphene · Interfacial adhesion · Antibacterial activities · Electrical conductivity

✉ Shih-Hsuan Chiu
schiu@mail.ntust.edu.tw

1 Department of Materials Science and Engineering, National Taiwan University of Science and Technology, Taipei, Taiwan 10607, Republic of China

2 Department of Materials Science and Engineering, Vanung University, Jongli, Taoyuan, Taiwan 32061, Republic of China

3 Department of Creative Fashion Design, Taoyuan Innovation Institute of Technology, Jongli, Taoyuan, Taiwan 32091, Republic of China

4 Institute of Materials Science and Engineering, Material Corrosion and Protection Key Laboratory of Sichuan Province, Sichuan University of Science and Engineering, Zigong 643000, China

5 Faculties of Biological and Chemical Engineering, Faculties of Materials Engineering, Science and Technology Innovation Center, Panzhihua University, Panzhihua 617000, China

Introduction

Polyurethanes (PUs) are a functional elastomer which can be synthesized from different raw materials. Attributes of PUs contain abrasion resistance, damping, flexibility, elasticity and chemical resistance [1]. Due to such characteristics, PUs have been widely investigated for industrial applications, including use in adhesives, paint, medical equipment and textile industry [2–6].

In recent years, due to rise of environmental consciousness, many researchers actively work on biodegradable polymers. Generally speaking, easily hydrolysable soft segments contain polylactic acid (PLA), polyglycolic acid (PGA), polycaprolactone (PCL) and polyacrylic acid (PAA) and so on [7–12]. They all have biocompatibility advantages. PCLs are soft segments which are usually applied to PU. However, many research results show that PCL of high content is beneficial to the increase of molecular weight and hydrolytic degradation of PU [13–18].

$\textcircled{2}$ Springer

Organic/inorganic nanocomposites subject to considerable concern in academic and industrial fields. Inorganic filler contains clay, graphene, fibreglass, carbon and carbon black. These reinforcing materials are used for reinforcing polymer materials [19, 20]. In which, graphene is a novel material and subjects to considerable researches in various fields. Graphene has been proven to be the thinnest and strongest substance at present. Graphene is hard and flexible and has superior thermal and electric conduction [21–23]. The mechanical property of graphene is 100 times stronger than iron and steel, and the electronic mobility and thermal conductivity of graphene are the highest among all materials. These excellent properties of graphene can be integrated with polymers, and properties of the polymers will be greatly improved [24–33]. For example, Yadav et al. prepare high-performance graphene/nanocomposites by using in situ polymerization. Results exhibit that functionalized graphene leads to good dispersion in a polymer matrix. When 2 wt% of graphene is added, the elastic modulus of PU is improved by 10 times by the graphene, and the thermal stability of PU is improved. The mechanical property and thermal property of polymers are obviously improved, and the polymers have outstanding shape recovery [27]. Cai et al. research that graphene oxide achieves good dispersity in PU, and such a result can improve the mechanical property and thermal property of PU [28]. When the amount of GO added is 4 wt%, the Young's Modulus of PU is improved by seven times. Kuila synthesizes graphene/poly(methyl methacrylate) (PMMA) nanocomposites. DMA, DSC and TGA analyses represents that the thermal property of PMMA is greatly improved by adding the graphene [30]. Silver nanoparticles have been medically known as an antibacterial agents and can serve as paint for a medical treatment machine [34]. Silver nanoparticles are also used as a biomaterial and are applied to tissue engineering [35]. Silver nanoparticles have bactericidal effects on *Staphylococcus aureus* and *Escherichia coli* [36]. In existing researches, silver nanoparticles, silver oxide and silver salts are added into a polymer matrix, so as to provide antimicrobial/biocidal activities [37–39].

To sum up, the physical property of polymers can be improved through adding graphene, and the polymers can be endowed with antibacterial properties by the silver nanoparticles. Therefore, in this study, the graphene is firstly plated with the silver nanoparticles, so as to form a silver nanoparticle/graphene material (Ag/G). However, as far as we know, no published news about biodegradable PCL-based PUs and Ag/G exists. Therefore, the influence on the mechanical properties caused by interfacial adhesion between Ag/G and PU will be researched in this study. The effect of different content of Ag/G on the structure, morphology, thermal properties, mechanical properties, hydrophobicity, antibacterial performance and electrical resistance of the PU was investigated.

Experimental

Synthesis of Ag/G/PU nanocomposites

4,4′-Diphenylmethane diisocyanate (MDI), polycaprolactone diol (PCL, Mn = 530) (PCL) and 1,4-butane diol were purchased from Aldrich. *N,N*-dimethylacetamide (DMAc) was obtained from Mallinckrodt Chemicals. Ag/G was purchased from Apex Nanotek Corporation. The specific surface area, oxygen content and average thickness for graphene were 25 m^2/g, <3 wt% and 5 nm, respectively. The average particle size of nano silver was <100 nm dispersions.

In this experiment, polycaprolactone (PCL) as a soft segments and 4,4,-diphenylmethane diisocyanate (MDI) used as a hard segment were dissolved in DMAc. While mixing with a mechanical mixer at a speed of 300 rpm, the mixture was reacted for 2 h at 75 °C forming a prepolymer. The chain extender 1,4-butanediol (1,4-BD) was then added and reacted for another 1 h to form polyurethane (Scheme 1). The Ag/G/DMAc solution was then dispersed in an ultrasound oscillator and added to the freshly synthesized polyurethane solution in the reactor at 75 °C and stirred by a mechanical mixer. The speed of the mechanical mixer was increased to 600 rpm to blend the mixture for another 1 h. Ag/G/PUs nanocomposites were finally obtained. The formulation of the soft and hard segments for PU and the proportion of added Ag/G are shown in Table 1. The molecular weight distribution of PU relative to polystyrene standards was measured using a gel permeation chromatographer (Jasco model PU-2080 plus) with tetrahydrofuran as a carrier solvent. The weight average molecular weight (Mw) of PU was 64,323 g/mole with a polydispersity index of 1.4.

Gel permeation chromatography (GPC)

A gel permeation chromatograph (Analytical Scientific Instruments Model 500) with a reflection index (RI) detector (Schambeck RI2000) and two columns in a series consisting of a Jordi gel DVB mixed bed and a 10,000 Å bed at 30 °C was used to measure the molecular weight distribution relative to polystyrene standards. The calibration curve was obtained using eight standards with molecular weights ranging from 3420 to 2.57×10^6. Tetrahydrofuran was used as the carrier solvent at a flow rate of 1 ml/min.

Transmission electron microscopy analysis

A transmission electron microscope (TEM, Hitachi model H-7500) was used to examine the morphology of the Ag/G/PUs nanocomposites. The samples for TEM examination were first prepared by placing the nanocomposite films into epoxy capsules and curing the epoxy at 70 °C for 24 h in an oven. The cured epoxies containing Ag/G/PUs nanocomposites were then microtomed with a diamond knife into 70–90-nm-thick

Scheme 1 Synthesis formula for the PU
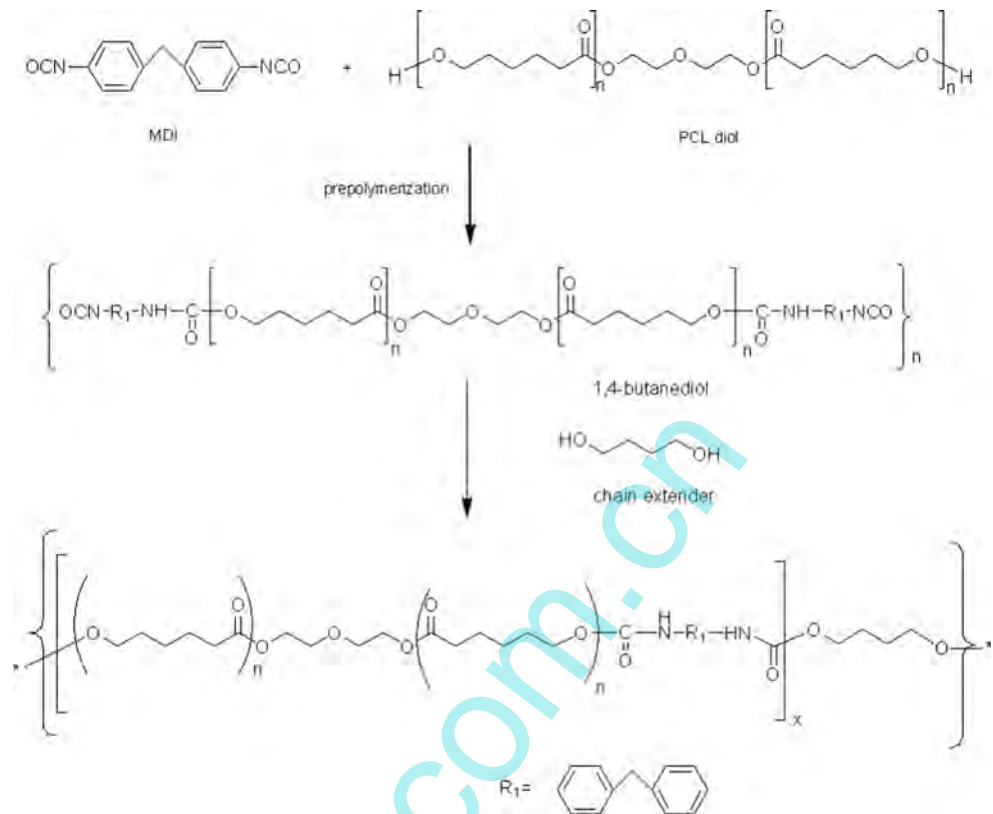
slices at −100 °C. Finally, a 3-nm-thick carbon layer was deposited on the slices placed on 200-mesh copper grids for TEM observation.

Morphology analysis

The morphology of the specimens at tensile fracture surfaces was observed by using a Hitachi scanning electron microscope (SEM), model SU1510. Specimens of 2×2 cm^2 were fixed on a sample holder using conductive adhesive tape and were subsequently coated with a thin layer of gold to improve the image resolution. The samples were photographed at 1 or 3 K magnification.

Fourier transform infrared spectroscopy (FT-IR)

FT-IR measurements were performed using a PerkinElmer spectrometer (model Spectrum One). Spectra of the samples were obtained by averaging 16 scans with a wavenumber range of 4000 to 650 cm^{-1} and a resolution of 2 cm^{-1}.

Energy-dispersive X-ray spectroscopy (EDS)

Elemental compositions of the Ag/G/PUs nanocomposites were examined using an energy-dispersive X-ray spectroscopy analyser (Horiba, model 7021-H). Specimens of 2×2 cm^2 were fixed on a sample holder using conductive adhesive tape and were then coated with a thin layer of gold to improve the image resolution. The samples were photographed at 1 K magnification.

X-ray diffraction (XRD)

X-ray diffraction was performed using a Rigaku diffractometer (model RU-H3R). The X-ray beam used Ni-filtered CuKa radiation from a sealed tube operated at 60 kV and 300 mA. Data were obtained in the 2θ range of 10°–70° with a scanning interval of 0.05°.

Table 1 Formulas of the Ag/G/PUs nanocomposites

Designation	MDI (moles)	PCL (moles)	1,4-BD (moles)	Ag/G (wt%)
PU	4	3.0	1.0	0
Ag/G/PU-01	4	3.0	1.0	0.05
Ag/G/PU-02	4	3.0	1.0	0.1
Ag/G/PU-03	4	3.0	1.0	0.2

Thermogravimetric analysis (TGA)

Thermogravimetric analysis was performed using a thermogravimetric analyser (PerkinElmer, model Pyris 1). Samples (5–8 mg) were heated from room temperature to 700 °C under nitrogen at a rate of 10 °C/min.

Differential scanning calorimetry (DSC)

Differential scanning calorimetry was performed on a PerkinElmer DSC, model Jade. Samples were sealed in aluminium pans with a perforated lid. The scans (−50 to 200 °C) were performed with a heating rate of 10 °C/min under nitrogen purging. The glass transition temperatures (T_g) can be located as the midpoints of sharp descent regions in the recorded curves. Samples of approximately 5–8 mg were used for all tests.

Dynamic mechanical analysis (DMA)

Dynamic mechanical analysis was performed using a SEIKO analyser (model SII Muse, DMS6100) at 1 Hz with a 5 μm amplitude over a temperature range of −50 to 40 °C and at a heating rate of 3 °C/min. DMA was conducted using tension mode and specimen dimensions of 20 mm × 5 mm × 0.2 mm (L × W × H). T_g was taken as the peak temperature of the glass transition region in the tan δ curve.
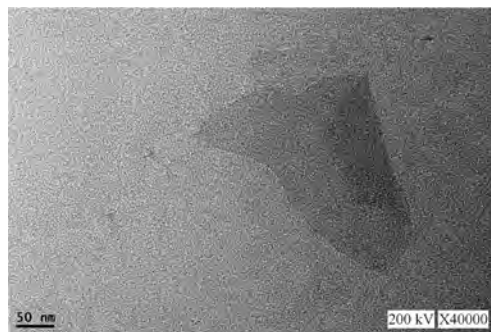
Fig. 2 TEM micrographs of the Ag/G/PU-03 nanocomposite

Stress-strain testing

Tensile strength and elongation at break were measured using a universal testing machine (MTS QTEST5, model QC505B1). Testing was conducted according to ASTM D638 specifications. The dimension of the film specimens was 45 mm × 8 mm × 0.2 mm.

Surface roughness analysis

Atomic force microscopy (AFM) scans were performed using a CSPM5500 instrument from Being Nano-instruments. Generally, there are two types of imaging modes, i.e., tapping and contact modes. Tapping mode was used in this study such that the oscillating probe cantilever
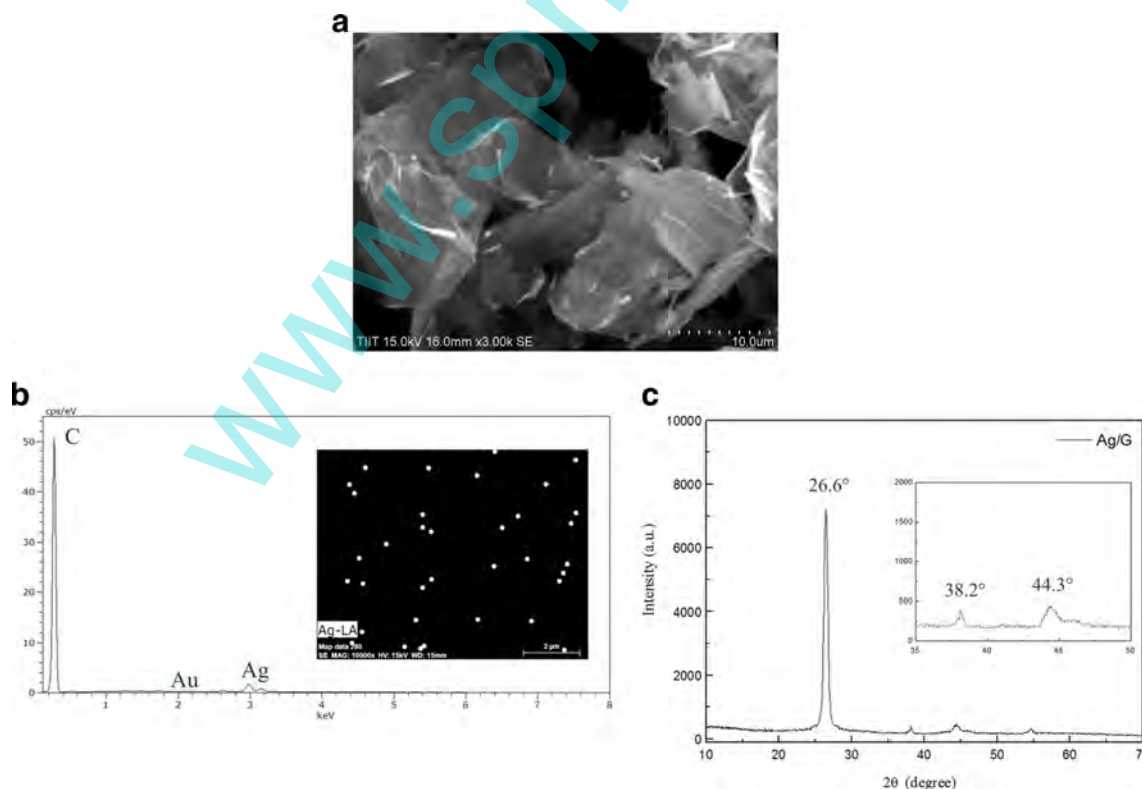
Fig. 1 Characterization of Ag/G: **a** SEM micrograph; **b** EDS image; and **c** XRD diffraction pattern

causes the tip to make only intermittent contact with the sample. With respect to the phase of the sine wave driving the cantilever, the phase of the tip oscillation is highly sensitive to various sample surface characteristics. Therefore, the tip can also sense the phase images of the sample surface in addition to the topography. The specimens were cut from Ag/G/PUs nanocomposite films with different clay contents.

Contact angle

Contact angles between the samples and deionized water were measured using a Face instrument (model CA-VP150) at room temperature. Dynamic advancing and receding contact angles were recorded while water was added to and withdrawn from the drop, respectively, using a syringe pump. Each reported contact angle is the average value from 3 to 4 drops.

Fig. 3 SEM photographs of fractured section of the Ag/G/PUs nanocomposites: **a** PU; **b** Ag/G/PU-01; **c** Ag/G/PU-02; and **d** Ag/G/PU-03 at 1000 magnification; **e** PU; **f** Ag/G/PU-01; **g** Ag/G/PU-02; and **h** Ag/G/PU-03 at 3000 magnification
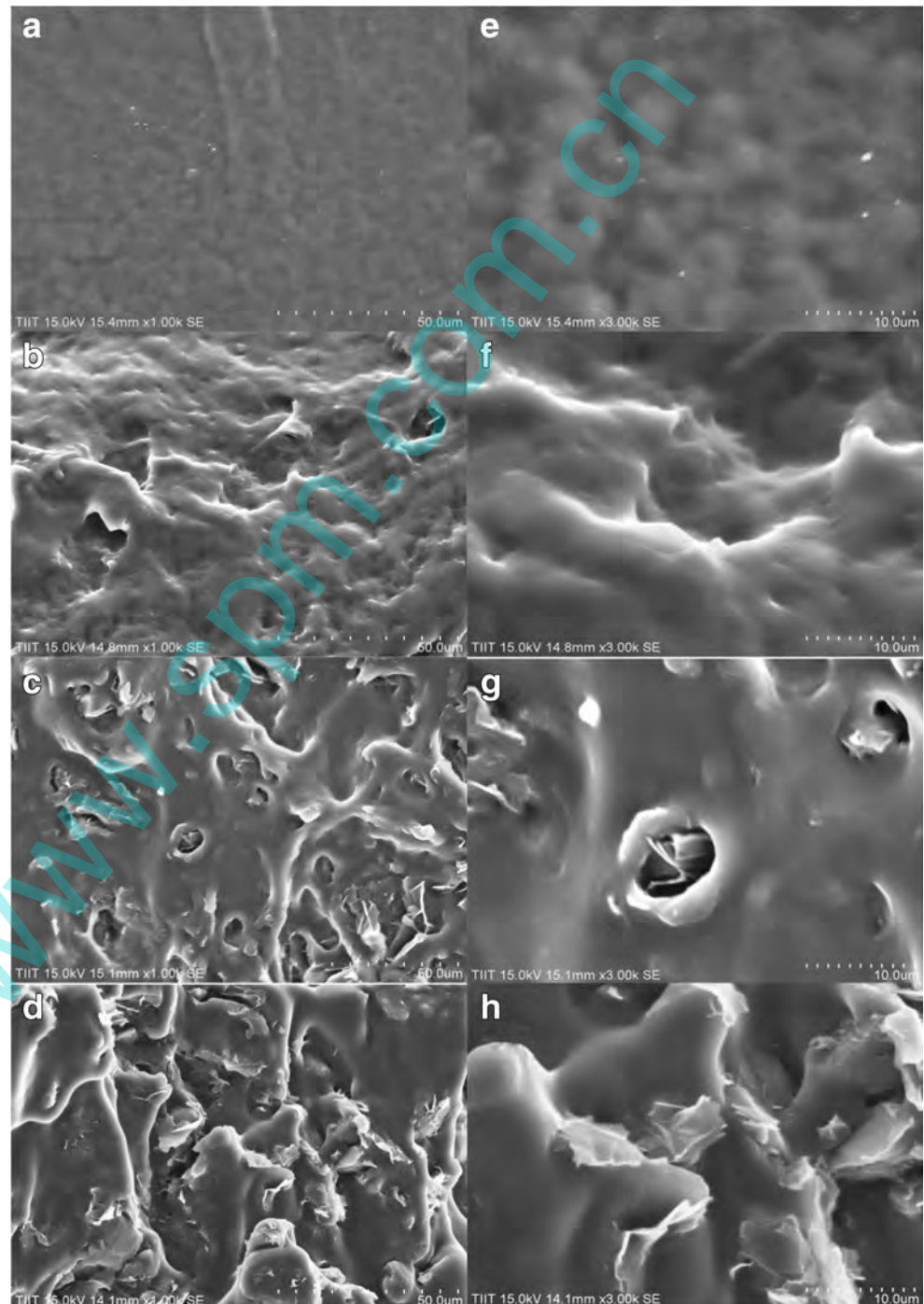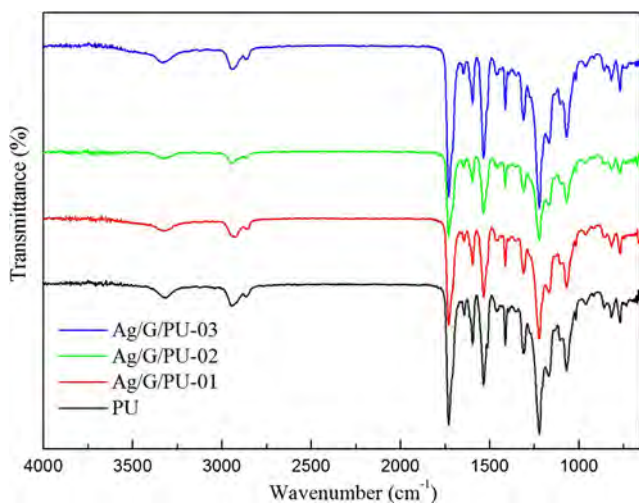
Fig. 4 FT-IR spectra of the Ag/G/PUs nanocomposites

Antibacterial evaluation

The antibacterial activity of the Ag/G/PUs nanocomposite was tested against aerobic bacteria commonly found on burn wounds: e.g., *S. aureus* (ATCC 25023) and *E. coli*. The assessment was conducted based on the disc diffusion method of the US Clinical and Laboratory Standards Institute (CLSI). The Ag/G/PUs nanocomposite was cut into circular discs (15 mm in diameter). Each specimen was placed on the Difco™ Mueller Hinton agar in a Petri dish, then the microbes therein were incubated at 37 °C for 24 h. If inhibitory concentrations were reached, there would be no growth of the microbes, which could be seen as a clear zone around the specimen discs. The clear zones were photographed.
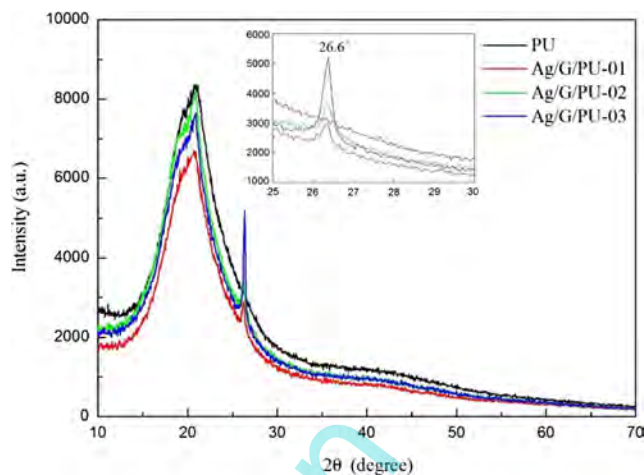
Fig. 6 XRD patterns of the Ag/G/PUs nanocomposites

Surface and volume conductivity analysis

An electrical resistance meter (Monroe Electronics, model 272A) was used to measure the surface and volumetric electrical resistances of Ag/G/PUs nanocomposite films at room temperature. The dimensions of the specimens were approximately 68 mm in diameter and 0.3 mm in thickness.

Results and discussion

Characterization of Ag/G

Figure 1 exhibits characterization of Ag/G. Referring to Fig. 1a, a sheet structure of Ag/G can be observed, and white
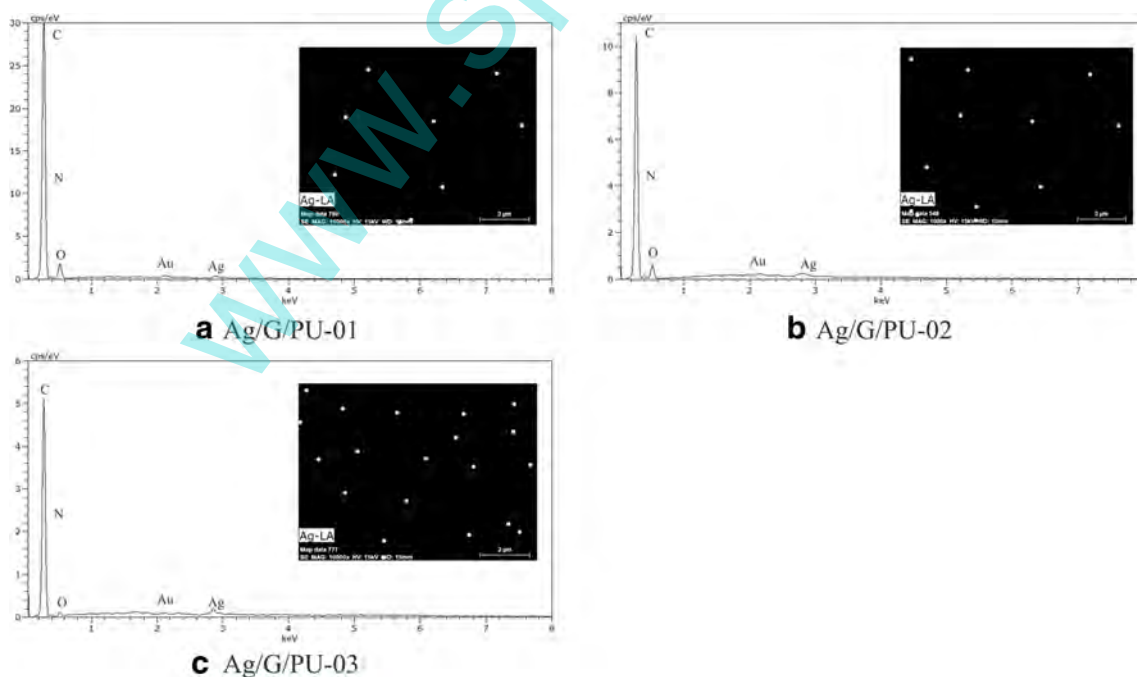
Fig. 5 EDS images of the Ag/G/PUs nanocomposites: **a** Ag/G/PU-01; **b** Ag/G/PU-02; and **c** Ag/G/PU-03
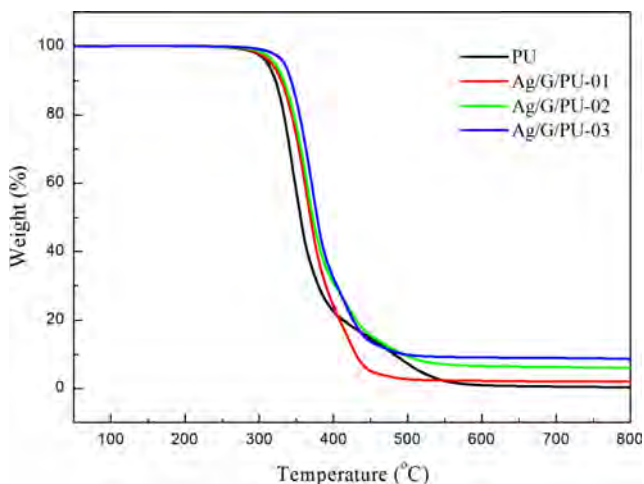
Fig. 7 TGA curves of the Ag/G/PUs nanocomposites
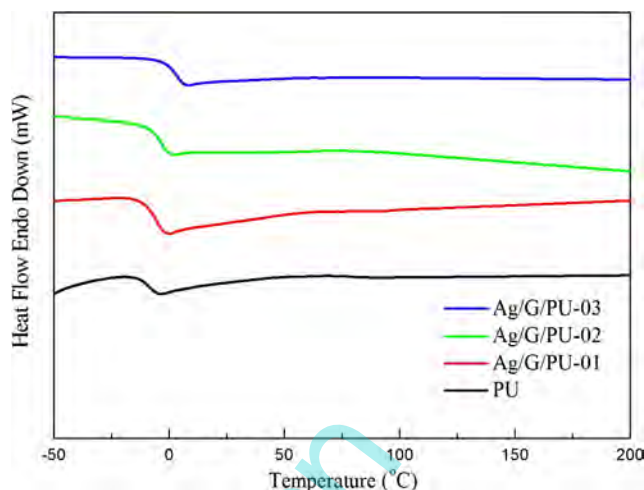
Fig. 8 DSC thermograms of the Ag/G/PUs nanocomposites

spots distributed on graphene nanosheets are silver nanoparticles. In addition, we can analyse from EDS in Fig. 1b that the silver content of Ag/G nanosheets is 10.72%. Figure 1c is an XRD spectrum of Ag/G, the sharp peak located at 26.6° for graphite [40, 41]. The Ag/G exhibits the obvious peaks at $2\theta = 38.2°$ and $44.3°$, which are due to the face-centred cubic crystalline silver, corresponding to the crystal faces of (111) and (200) [42, 43]. These results indicate the presence of Ag in Ag/G that was prepared by the Apex Nanotek Corporation through a certain nanotechnology.

Structure and morphology of Ag/G/PUs nanocomposites

In this study, Ag/G is mixed into a PU matrix by a solution dispersion method, so as to form Ag/G/PUs nanocomposites. Figure 2 shows the TEM micrograph of Ag/G/PU-03 nanocomposites. It is observed that the morphology of Ag/G belongs to nanosheet structures. The thickness size is smaller than 100 nm, and the diameter is of micrometre scale. This phenomenon means that the interfacial adhesion between Ag/G and PU is good, and the basic physical properties of PU can be strengthened.

The tensile fracture surfaces of Ag/G/PUs nanocomposites are shown in Fig. 3a–f. Mark numbers (a) to (d) are of 1000 magnification, and mark numbers (e) to (h) are of 3000 magnification. Panels a and e of Fig. 3 are fractured surfaces of PU, exhibiting a few wrinkles. The extruded wrinkles may be

the hard segment-rich phases. Panels b and f of Fig. 3 are Ag/G/PU-01 nanocomposite fracture surface with a small amount of Ag/G added. It is observed that the wrinkles of the fractured surfaces of PU become obvious when a small amount of Ag/G is added. In Fig. 3c, d, g, h, Ag/G nanosheets are further added into the PU matrix. It may be found that the wrinkles of the fractured surfaces of Ag/G/PUs become even more acute along with the increase of Ag/G contents. In addition, the Ag/G nanosheets and the PU matrix exhibit good dispersity and interfacial adhesion. Due to the phenomenon, we expect that the mechanical property of the PU matrix can be improved by adding the Ag/G.

The FT-IR spectra of the Ag/G/PUs nanocomposites are shown in Fig. 4. These four polymers exhibit similar functional groups and five major peaks, i.e., the NH stretching vibration peak group at 3314 cm^{-1}. The stretching vibration peaks of the alkyl C-H group are at 2942 and 2862 cm^{-1}, and carbonyl group (C=O) is nearby 1728. The peaks at 1642 and 1593 cm^{-1} belong to C=C stretching vibrations. C-O stretching vibrations peak appears nearby 1217 cm^{-1}. Furthermore, in this spectrum, no free NCO group presents to 2240–2275 cm^{-1}. These results represent that NCO-terminated prepolymer fully reacts with 1,4-BD during synthesis.

Figure 5 shows the results of elemental analysis from the energy-dispersive X-ray spectra of the Ag/G/PUs nanocomposites. The contents of Ag measured in Ag/G/PU-01, Ag/G/

Table 2 Thermal properties of the Ag/G/PUs nanocomposites

Sample	TGA		DSC	DMA	
	T_{onset} (°C)	Residue at 800 °C	T_g (°C)	T_{gd} from tanδ(°C)	Tan δ_{max}
PU	320.1	0.3%	−9.2	−6.1	0.409
Ag/G/PU-01	331.3	1.9%	−6.2	−2.7	0.341
Ag/G/PU-02	335.1	6.0%	−3.3	−0.6	0.312
Ag/G/PU-03	341.7	8.6%	−2.5	4.2	0.291

Fig. 9 Tan δ curve of the Ag/G/PUs nanocomposites

Table 3   Tensile properties of the Ag/G/PUs nanocomposites

Sample	Tensile strengths (MPa)	Strain at break (%)
PU	16.9	1118
Ag/G/PU-01	22.2	1088
Ag/G/PU-02	25.5	944
Ag/G/PU-03	30.8	892

PUs nanocomposites: one crystalline Ag/G and the other amorphous PU. However, along with the increase of Ag/G contents, weak diffraction peaks of PU are free of obvious changes at $2\theta = 20°$ and are still amorphous.

Thermal properties of Ag/G/PUs nanocomposites

The TGA curves for the Ag/G/PUs nanocomposites are shown in Fig. 7. A first decomposition temperature is attributed to decomposition of urethane group. The onset temperatures, i.e., the initial decomposition temperatures of these polymers, are recorded in Table 2. The onset decomposition temperatures (T_{onset}) for PU, Ag/G/PU-01, Ag/G/PU-02 and Ag/G/PU-03 are 320.1, 331.3, 335.1 and 341.7 °C, respectively. Among these polymers, PU is free of any Ag/G nanosheets. Ag/G/PU-03 has the highest Ag/G nanosheets content. In addition, along with the increase of Ag/G nanosheets content, the content of decomposition temperature and residue of PU is increased at the same time. These results suggest that the thermal stability of PU can be improved along with the increase of Ag/G nanosheets content.

Figure 8 shows the DSC curves for the Ag/G/PUs nanocomposites. These results are summarized in Table 2. The T_g's determined from these thermograms for PU, Ag/G/PU-01, Ag/G/PU-02 and Ag/G/PU-03 are −9.2, −6.2, −3.3 and −2.5 °C, respectively. This result represents that the T_g of PU is increased at the same time along with the increase of Ag/G nanosheets content. The fact that Ag/G belongs to rigid structures hinders the segmental motion of PU. In a DSC curve, no typical of endothermic and exothermic crystallization peaks is observed among all polymers. This represents that PU is still amorphous by adding Ag/G nanosheets, and this is consistent with an XRD result.

Figure 9 shows the tan δ curves of Ag/G/PUs nanocomposites with different proportions of Ag/G nanosheets. Dynamic glass transition temperatures (T_{gd}) is defined at the peak of the tan δ curve. The T_{gd} values of PU, Ag/G/PU-01, Ag/G/PU-02 and Ag/G/PU-03 are −6.1, −2.7, −0.6 and 4.2 °C, respectively, and are summed up in Table 2. As the Ag/G content of the PU

PU-02 and Ag/G/PU-03 were 0.31, 0.65 and 1.14%, respectively. The Ag content increases with increasing Ag/G contents as anticipated. The weight percent of Ag is recorded in Table 5. The mapping suggests that the distribution of elemental Ag increased with increasing Ag/G contents.

The XRD spectra of the Ag/G/PUs nanocomposites are shown in Fig. 6. It may be found from a spectrogram that a weak diffraction peak of PU occurs when $2\theta = 20°$. This broad diffraction peak is an absorption peak of hard segments of PU [43]. Furthermore, the XRD patterns belong to an amorphous polymer for Ag/G/PUs. A single amorphous halo around 20° [44] for Ag/G/PUs with low hard segments content was obtained [45]. $2\theta = 20°$ and 26.6° occurs in Ag/G/PU-01, Ag/G/PU-02 and Ag/G/PU-03. Among characteristic crystallization peaks of $2\theta = 20°$, a sharp peak occurs at $2\theta = 26.6°$. In addition, the peak is increased along with the increase of Ag/G content. In virtue of that only a small amount of Ag/G was added to the PU matrix, the characteristic of Ag is not observed in the diffraction pattern of each nanocomposite. Thus, there are two kinds of morphologies in each Ag/G/

Fig. 10 Tensile properties of the Ag/G/PUs nanocomposites

Fig. 11 AFM 3D morphologies and phase images of the Ag/G/PUs ▶ nanocomposites with different Ag/G contents. Ag/G content: *A*, 0 wt %; *B*, 0.05 wt%; *C*, 0.1 wt %; *D*, 0.2 wt%. 3D morphology: *A2, B2, C2, D2*. Phase: *A1, B1, C1, D1*
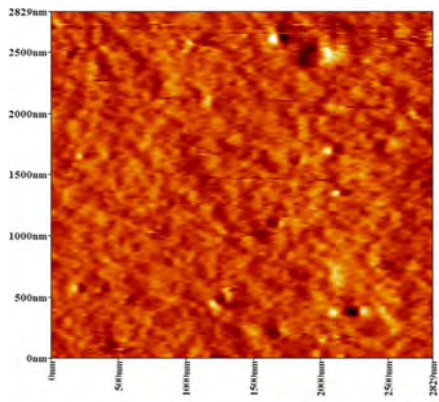
A1
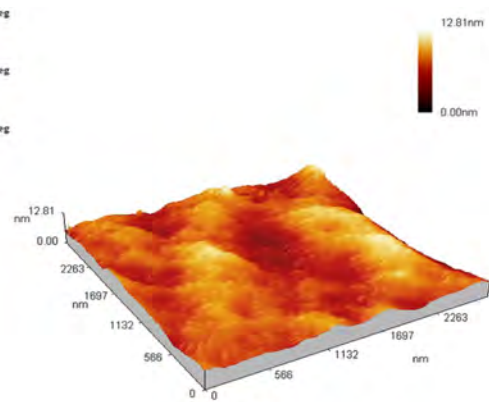
A2
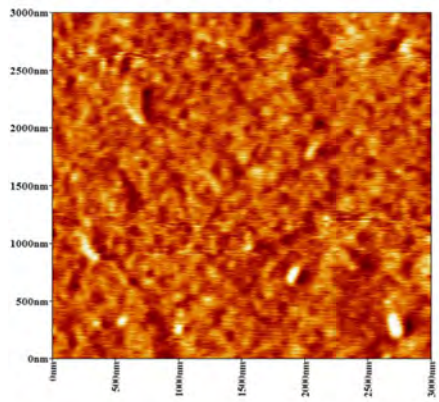
B1
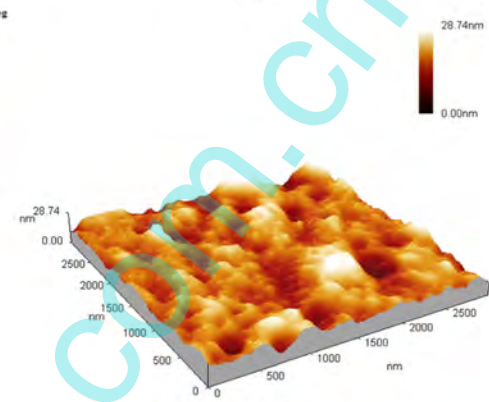
B2
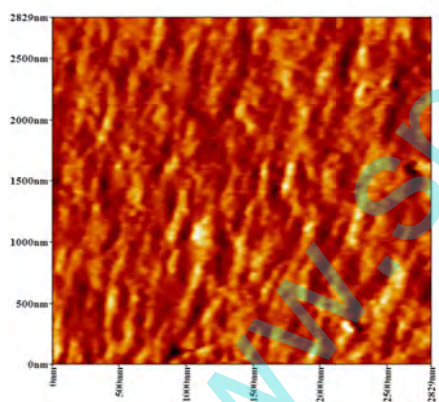
C1
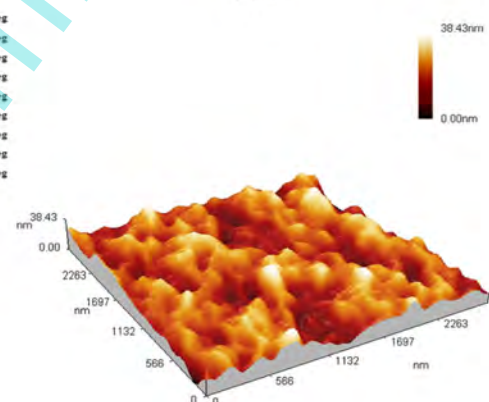
C2
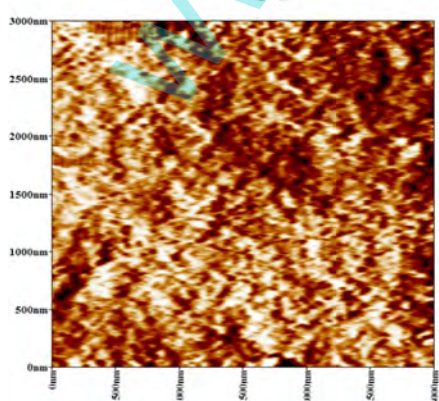
D1
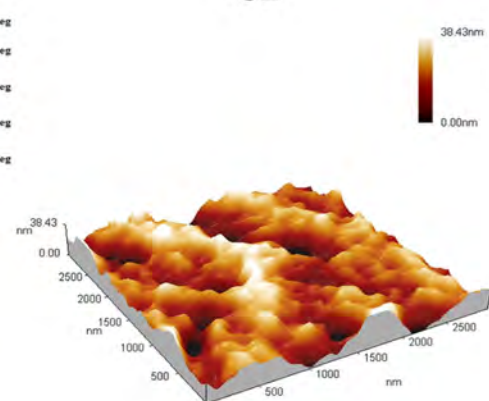
D2

Table 4 Surface roughness data of the Ag/G/PUs nanocomposites

Sample	Ra (nm)
PU	1.09
Ag/G/PU-01	2.72
Ag/G/PU-02	4.43
Ag/G/PU-03	6.58

increases, T_{gd} also increases. This result is consistent with the discussion on DSC. Meanwhile, through adding the Ag/G nanosheets, the peak of tan δ of PU is lowered at the same time. The PU with higher Ag/G content behaves more like elastic solid and less like viscous liquid. Therefore, PU containing the Ag/G nanosheets has a lower loss modulus and a higher storage modulus.

Mechanical properties of Ag/G/PUs nanocomposites

Figure 10 shows the stress-strain curves for Ag/G/PUs nanocomposites with different proportions of Ag/G nanosheets, and the results are listed in Table 3. The tensile strengths of PU, Ag/G/PU-01, Ag/G/PU-02 and Ag/G/PU-03 are 16.9, 22.2, 25.5 and 30.8 MPa, respectively. This result represents that by increasing Ag/G content, the tensile strength is improved at the same time. It can be observed from Fig. 3 that interfacial adhesion between PU and Ag/G of the Ag/G nanosheets is good. This phenomenon can reinforce the interfacial interaction between Ag/G and the PU matrix. On the other hand, the elongation at breaks of PU, Ag/G/PU-01, Ag/G/PU-02 and Ag/G/PU-03 were 1118, 1088, 944 and 892%, respectively. This result is obtained due to the fact that the

Ag/G nanosheets belong to rigid structures, are also unfavourable to the sliding motions between the polymer chains and further reduce the elongation at break of the polymer.

Surface properties of Ag/G/PUs nanocomposites

The 3D morphologies and phases for the Ag/G/PUs nanocomposites are shown in Fig. 11. It can be observed that the 3D morphologies and phases change after the Ag/G nanosheets are added to PU. The 3D morphologies exhibit that after the Ag/G nano sheets are added, surfaces of Ag/G/PU-01, Ag/G/PU-02 and Ag/G/PU-03 have obvious irregular projections. The phase image showed these polymers added Ag/G nanosheets. An abundance of isolated small domains has irregular granular or channel-like morphologies. In the phase image, continuous dark areas belong to PU soft segments. Bright areas are attributed to the hard segments. Moreover, the average roughness of PU, Ag/G/PU-01, Ag/G/PU-02 and Ag/G/PU-03 nanocomposites are 1.09, 2.72, 4.43 and 6.58 nm, respectively, and is listed in Table 4. These results represent that the surface roughness of the Ag/G/PUs nanocomposites is increased along with the increase of Ag/G content.

Figure 12 shows photographs and data of the contact angles measurements for the Ag/G/PUs nanocomposites. The contact angles for PU, Ag/G/PU-01, Ag/G/PU-02 and Ag/G/PU-03 are 75.3°, 76.9°, 83.3° and 87.1°, respectively. This result represents that the contact angle of the Ag/G/PUs nanocomposites will be increased by adding the Ag/G nanosheets. This can be attributed to results of AFM and the surface of PU can be of protrusions as lotus leaves by adding the Ag/G

Fig. 12 Surface properties of the Ag/G/PUs nanocomposites
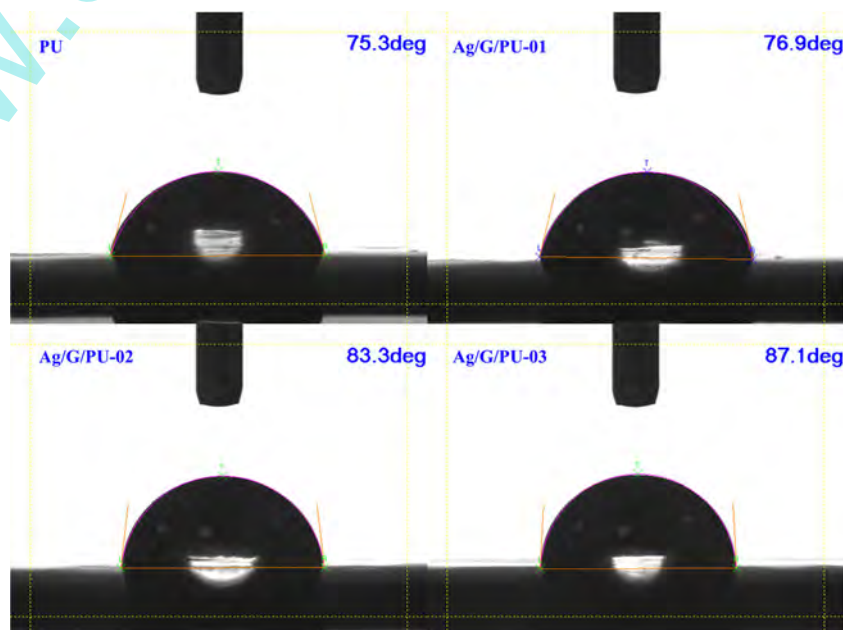
Fig. 13 Inhibition zone of Ag/G/
PUs nanocomposites for
S. aureus

a Ag/G/PU-01

b Ag/G/PU-02

c Ag/G/PU-03
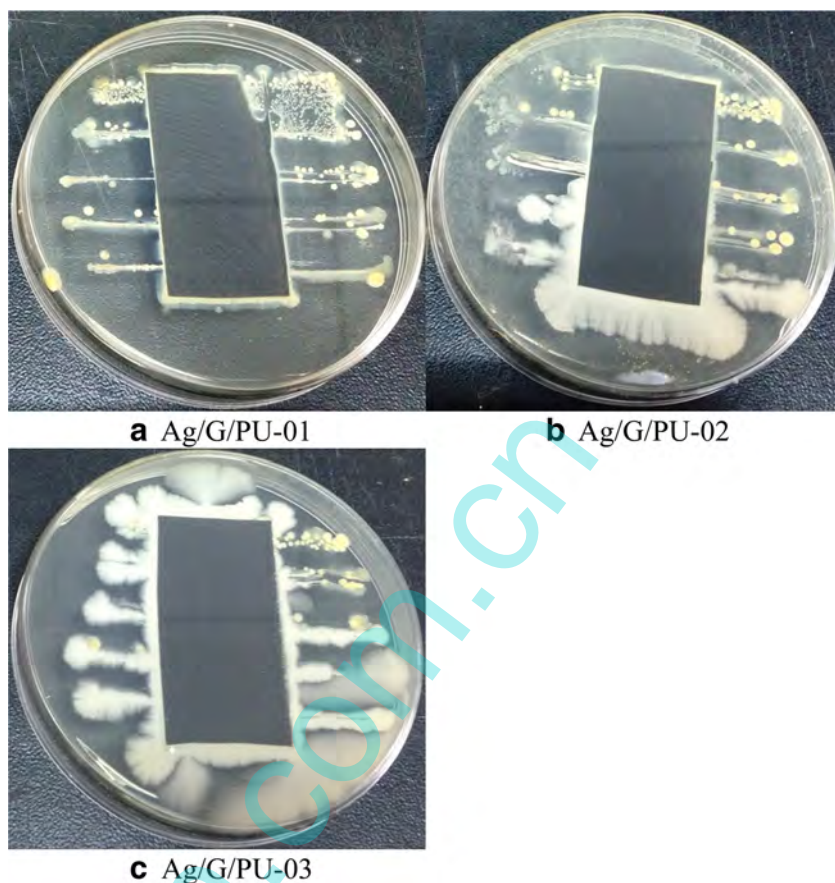
nanosheets. Due to these results, the surface roughness of the Ag/G/PUs nanocomposites can be increased, and thus, the hydrophobicity of PU is improved. Therefore, the Ag/G/PUs nanocomposites can have a high contact angle after the Ag/G nanosheets are added.

Antibacterial evaluation of Ag/G/PUs nanocomposites

Figure 13 lists the zone of inhibition toward *S. aureus* for the Ag/G/PUs nanocomposites. It may be observed that by adding the Ag/G nanosheets, *S. aureus* extends outwards from the edge of PU. The results show that the zone of inhibition

increases with increasing Ag/G nanosheets content. This indicates that the Ag/G provides the antibacterial activities for the Ag/G/PUs nanocomposites. In addition, Table 5 also exhibits the sterilization or antibacterial rates of Ag/G/PUs nanocomposites. For *S. aureus*, the antibacterial rates of the Ag/G/PU-01, Ag/G/PU-02, and Ag/G/PU-03 are 21.2, 39.0, and 60.1% in sequence. For *E. coli*, the results are similar, that the antibacterial rates of these polymers are 25.3, 47.9 and 55.6%, respectively. Therefore, Ag/G/PUs nanocomposites have antibacterial activities. The antibacterial rates are increased along with the increase of Ag/G nanosheets content.

Electrical resistance analysis of Ag/G/PUs nanocomposites

Figures 14 and 15 show the surface and volumetric electrical resistivity for the Ag/G/PUs nanocomposites. The surface electrical resistivity measured at 10 V for PU, Ag/G/PU-01, Ag/G/PU-02 and Ag/G/PU-03 was $3.7 \cdot 10^{13}$, $3.5 \cdot 10^{12}$, $1.7 \cdot 10^{12}$ and $5.0 \cdot 10^{10}$ Ω/cm^2, respectively. Those measured at 100 V for these nanocomposites were $3.7 \cdot 10^{13}$, $3.1 \cdot 10^{12}$, $2.4 \cdot 10^{11}$ and $1.1 \cdot 10^{10}$ Ω/cm^2 in sequence. Similarly, the volumetric electrical resistivity for PU, Ag/G/PU-01, Ag/G/PU-02 and Ag/G/PU-03 was $1.7 \cdot 10^{11}$, $3.7 \cdot 10^{10}$, $1.5 \cdot 10^{10}$ and $4.3 \cdot 10^{9}$ $\Omega \cdot cm$, respectively. Those measured at 100 V for these

Table 5 Ag content from antibacterial activity of the Ag/G/PUs nanocomposites

Sample	Ag (wt%)	Antibacterial ratio (%)	
		S. aureus	*Escherichia coli*
PU	–	Blank	Blank
Ag/G/PU-01	0.31	21.2	25.3
Ag/G/PU-02	0.61	39.0	47.9
Ag/G/PU-03	1.15	60.1	55.6
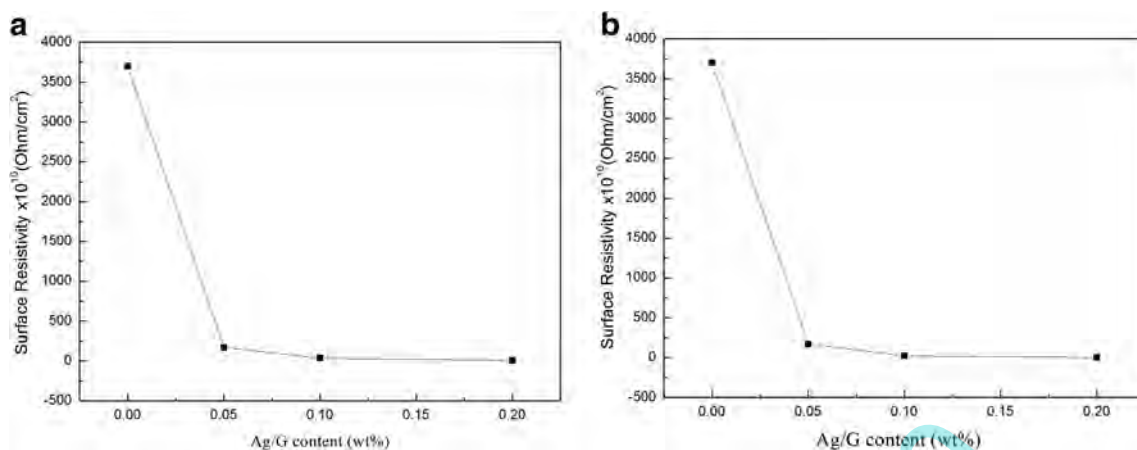
Fig. 14 Surface electrical resistivities of Ag/G/PUs nanocomposites: at **a** 10 V; **b** 100 V

polymers were $1.1 \cdot 10^{11}$, $3.6 \cdot 10^{10}$, $3.4 \cdot 10^{9}$ and $1.8 \cdot 10^{9}$ $\Omega \bullet$cm, correspondingly. These data represent that the surface and volumetric electrical resistivities of the Ag/G/PUs nanocomposites are lowered along with the increase of Ag/G content. In other words, conductivity is improved along with the increase of Ag/G contents. This is due to Ag/G nanosheets being slightly conductive materials.

Conclusions

Ag/G/PUs nanocomposites were successfully prepared in this paper. It can be observed from SEM, EDS and XRD that the surface of graphene is attached with silver nanoparticles. TEM analysis exhibits that Ag/G is of a sheet structure and has the thickness smaller than 100 nm. Tensile fractured surfaces of Ag/G/PUs nanocomposites can be found, and good interfacial adhesion, and there exists strong interface interaction between the Ag/G nanosheets and the PU matrix. FT-IR spectrum represents that MDI has been completely consumed. The EDS analysis exhibits that the content of Ag is increased along with the adding of the Ag/G nanosheets. XRD analysis exhibits that Ag/G/PUs nanocomposites are still amorphous along with the increase of Ag/G nanosheets content. Thermal analysis exhibits that the content of the Ag/G nanosheets is increased along with the increase of initial decomposition temperatures, T_g and T_{gd} of Ag/G/PUs nanocomposites. The tensile strength of the Ag/G/PUs nanocomposites increase with increasing Ag/G nanosheets content. On the contrary, elongation at break decreases with increasing Ag/G nanosheets content. The surface property of the Ag/G/PUs nanocomposites exhibits that the surface roughness and hydrophobicity of the Ag/G/PUs nanocomposites are improved along with the increase of Ag/G nanosheets content. Besides, the Ag/G/PUs nanocomposites have antibacterial activities toward *S. aureus* as well as *E. coli* and their antibacterial rates increase with increasing Ag/G nanosheets content. Furthermore, the surface and volumetric electrical resistivity for Ag/G/PUs nanocomposites decreased with increasing Ag/G nanosheets content.
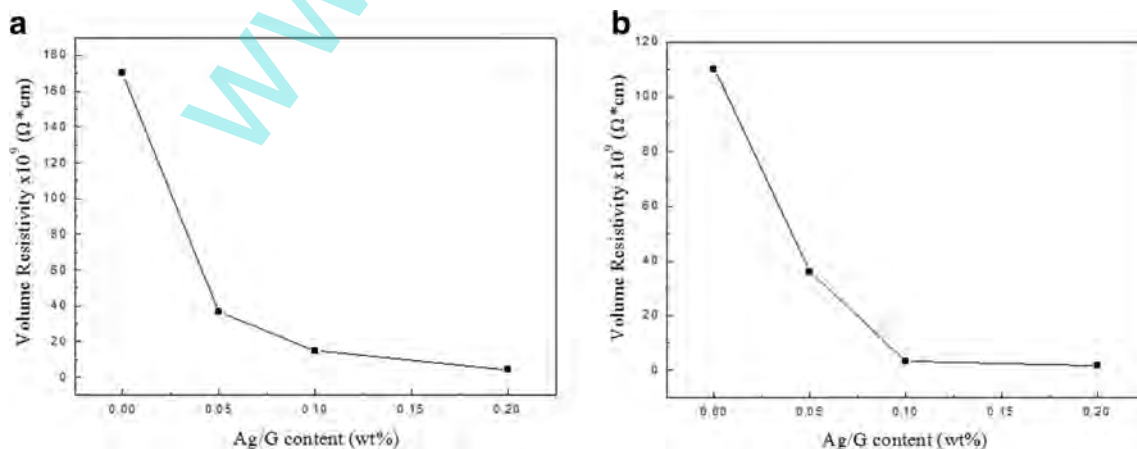
Fig. 15 Volumetric electrical resistivities of the Ag/G/PUs nanocomposites: at **a** 10 V; **b** 100 V

References

1. Wang CH, Auad ML, Marcovich NE, Nutt S (2008) Synthesis and characterization of organically modified attapulgite/polyurethane nanocomposites. J Appl Polym Sci 109:2562–2570

2. Gugliuzza A, Clarizia G, Golemme G, Drioli E (2002) New breathable and waterproof coatings for textiles: effect of an aliphatic polyurethane on the formation of PEEK-WC porous membranes. Eur Polym J 38:235–242

3. Tien YI, Wei KH (2001) Hydrogen bonding and mechanical properties in segmented montmorillonite/polyurethane nanocomposites of different hard segment ratios. Polymer 42:3213–3221

4. Park HB, Lee YM (2002) Separation of toluene/nitrogen through segmented polyurethane and polyurethane urea membranes with different soft segments. J Membr Sci 197:283–296

5. Abraham GA, de Queiroz AAA, San Roman JS (2001) Hydrophilic hybrid IPNs of segmented polyurethanes and copolymers of vinylpyrrolidone for applications in medicine. Biomaterials 22: 1971–1985

6. Mequanint K, Sanderson R (2003) Nano-structure phosphorus-containing polyurethane dispersions: synthesis and crosslinking with melamine formaldehyde resin. Polymer 44:2631–2639

7. Okada M (2002) Chemical syntheses of biodegradable polymers. Prog Polym Sci 27:87–133

8. Coulembier O, Degee P, Hedrick JL, Dubois P (2006) From controlled ring-opening polymerization to biodegradable aliphatic polyester: especially poly(betamalic acid) derivatives. Prog Polym Sci 31:723–747

9. Huang SJ (1985) Encyclopedia of polymer science and engineering 2:220-243

10. Nair LS, Laurencin CT (2007) Biodegradable polymers as biomaterials. Prog Polym Sci 32:762–798

11. Pena J, Corrales T, Izquierdo-Barba I, Doadrio AL, Vallet-Regi M (2006) Long term degradation of poly(ε-caprolactone) films in biologically related fluids. Polym Degrad Stab 91:1424–1432

12. Chandra R, Rustgi R (1998) Biodegradable polymers. Prog Polym Sci 23:1273–1335

13. Tatai L, Moore TG, Adhikari R, Malherbe F, Jayasekara R, Griffiths I (2007) Thermoplastic biodegradable polyurethanes: the effect of chain extender structure on properties and in-vitro degradation. Biomaterials 28:5407–5417

14. Heijkants RGJC, Schwab LW, van Calck RV, de Groot JH, Pennings AJ, Schouten AJ (2005) Extruder synthesis of a new class of polyurethanes: polyacylurethanes based on poly(ε-caprolactone) oligomers. Polymer 46:8981–8989

15. Li FG, Hou JN, Zhu W, Zhang XA, Xu M, Luo XL (1996) Crystallinity and morphology of segmented polyurethanes with different soft-segment length. J Appl Polym Sci 62:631–638

16. Jiang X, Li JH, Ding MM, Tan H, Ling QY, Zhong YP (2007) Synthesis and degradation of nontoxic biodegradable waterborne polyurethanes elastomer with poly(ε-caprolactone) and poly(ethylene glycol) as soft segment. Eur Polym J 43:1838–1846

17. Ayres E, Oréfice RL, Yoshida MI (2007) Phase morphology of hydrolysable polyurethanes derived from aqueous dispersions. Eur Polym J 43:3510–3521

18. Tsou CH, Lee HT, Tsai HA, Cheng HJ, Suen MC (2013) Synthesis and properties of biodegradable polycaprolactone/polyurethanes by using 2,6-pyridinedimethanol as a chain extender. Polym Degrad Stab 98:643–650

19. Jeong EH, Yang J, Lee HS, Seo SW, Baik DH, Kim J, Youk JH (2008) Effective preparation and characterization of montmorillonite/poly(ε-caprolactone)-based polyurethane nanocomposites. J Appl Polym Sci 107:803–809

20. Chen H, Lu H, Zhou Y, Zheng M, Ke C, Zeng D (2012) Study on thermal properties of polyurethane nanocomposites based on organosepiolite. Polym Degrad Stab 97:242–247

21. Li D, Muller MB, Gilje S, Kaner RB, Wallace GG (2008) Processable aqueous dispersions of graphene nanosheets. Nat Nanotechnol 3:101–105

22. Stankovich S, Piner RD, Chen XQ, Wu NQ, Nguyen ST, Ruoff RS (2006) Stable aqueous dispersions of graphitic nanoplatelets via the reduction of exfoliated graphite oxide in the presence of poly(sodium 4-styrenesulfonate). J Mater Chem 16:155–158

23. Allen MJ, Tung VC, Kaner RB (2010) Honeycomb carbon: a review of graphene. Chem Rev 110:132–145

24. Scognamillo S, Gioffredi E, Piccinini M, Lazzari M, Alzari V, Nuvoli D, Sanna R, Piga D, Malucelli G, Mariani A (2012) Synthesis and characterization of nanocomposites of thermoplastic polyurethane with both graphene and graphene nanoribbon fillers. Polymer 53:4019–4024

25. Cai D, Jin J, Yusoh K, Rafiq R, Song M (2012) High performance polyurethane/functionalized graphene nanocomposites with improved mechanical and thermal properties. Compos Sci Technol 72:702–707

26. Kumar M, Chung JS, Kong BS, Kim EJ, Hur SH (2013) Synthesis of graphene–polyurethane nanocomposite using highly functionalized graphene oxide as pseudo-crosslinker. Mater Lett 106:319–321

27. Yadav SK, Cho JW (2013) Functionalized graphene nanoplatelets for enhanced mechanical and thermal properties of polyurethane nanocomposites. Appl Surf Sci 266:360–367

28. Cai D, Jin J, Yusoh K, Rafiq R, Song M (2012) High performance polyurethane/functionalized graphene nanocomposites with improved mechanical and thermal properties. Combust Sci Technol 72:702–707

29. Liao KH, Qian Y, Macosko CW (2012) Ultralow percolation graphene/polyurethane acrylate nanocomposites. Polymer 53: 3756–3761

30. Kuila T, Bose S, Khanra P, Kim NH, Rhee KY, Lee JH (2011) Characterization and properties of in situ emulsion polymerized poly(methyl methacrylate)/graphene nanocomposites. Compos Part A 42:1856–1861

31. Wang X, Weiyi X, Lei S, Yang H, Hu Y, Yeoh GH (2012) Fabrication and characterization of graphene-reinforced waterborne polyurethane nanocomposite coatings by the sol–gel method. Surf Coat Technol 206:4778–4784

32. Lee SK, Kim BK (2014) Synthesis and properties of shape memorygraphene oxide/polyurethane chemical hybrids. Polym Int 63:1197–1202

33. Oh SM, Oh KM, Dao TD, Lee H, Jeong HM, Kimb BK (2013) The modification of graphene with alcohols and its use in shape memory polyurethane composites. Polym Int 62:54–63

34. Holder IA, Durkec P, Supp AP, Boyce ST (2013) Assessment of a silver coated barrier dressing for potential use with skin grafts on excised burns. Burns 29:445–448

35. Venkateswarlu K, Rameshbabu N, Bose AC, Muthupandi V, Subramanian S, MubarakAli D, Thajuddin N (2012) Fabrication of corrosion resistant, bioactive and antibacterial silver substituted bydroxyapatite/titania composite coating on Cp Ti. Ceram Int 38: 731–740

36. Kumar A, Vemula PK, Ajayan PM, John G (2008) Silver-nanoparticle-embedded antimicrobial paints based on vegetable oil. Nat Mater 7:236–241

37. Hung HS, Hsu SH (2007) Biological performances of poly(ether)urethane-silver nanocomposites. Nanotechnology 18

38. Wang Y, Zhang Q, Fu Q (2003) Compatibilization of immiscible poly(propylene)/polystyrene blends using clay. Macromol Rapid Commun 24:231–235

39. Prabhakar PK, Raj S, Anuradha PR, Sawant SN, Doble M (2011) Biocompatibility studies on polyaniline and polyaniline–silver

nanoparticle coated polyurethane composite. Colloids Surf B 86: 146–153

40. Zhang K, Zhang Y, Wang S (2013) Enhancing thermoelectric properties of organic composites through hierarchical nanostructures. Sci Rep 3:3448–3454

41. Kun Z, Yue Z, Shiren W (2013) Enhancing thermoelectric properties of organic composites through hierarchical nanostructures. Sci Rep 3:3448

42. Cho JW, So JH (2006) Polyurethane-silver fibers prepared by infiltration and reduction of silver nitrate. Mater Lett 60:2653–2656

43. Zhang Z, Zhang L, Wang S, Chen W, Lei Y (2001) A convenient route to polyacrylonitrile/silver nanoparticle composite by simultaneous polymerization–reduction approach. Polymer 42:8315–8318

44. Crawford DM, Bass RG, Haas TW (1998) Strain effects on thermal transitions and mechanical properties of thermoplastic polyurethane elastomers. Thermochim Acta 323:53–61

45. Vilas JL, Laza JM, Rodríguez C, Rodríguez M, León LM (2013) New polyurethane-based magnetostrictive composites: dynamical mechanical properties. Polym Eng Sci 53:744–751